



Published in final edited form as:

Cancer Res. 2010 May 15; 70(10): 4045–4053. doi:10.1158/0008-5472.CAN-09-4414.

Preclinical Evaluation of an ¹³¹I-Labeled Benzamide for Targeted Radiotherapy of Metastatic Melanoma

John L. Joyal¹, John A. Barrett¹, John C. Marquis¹, Jianqing Chen¹, Shawn M. Hillier¹, Kevin P. Maresca¹, Marie Boyd², Kenneth Gage³, Sridhar Nimmagadda³, James F. Kronauge¹, Matthias Friebe⁴, Ludger Dinkelborg⁴, James B. Stubbs⁵, Michael G. Stabin⁶, Rob Mairs², Martin G. Pomper³, and John W. Babich¹

¹Molecular Insight Pharmaceuticals, Cambridge, MA, USA ²University of Glasgow, Glasgow, Scotland ³Johns Hopkins Medical Institutions, Baltimore, MD, USA ⁴Bayer Schering Pharma AG, Global Drug Discovery, Berlin, Germany ⁵Radiation Dosimetry Services, Charlotte, VA ⁶Vanderbilt University, Nashville, TN

Abstract

Radiolabeled benzamides are attractive candidates for targeted radiotherapy of metastatic melanoma as they bind melanin and exhibit high tumor uptake and retention. One such benzamide, *N*-(2-diethylamino-ethyl)-4-(4-fluoro-benzamido)-5-iodo-2-methoxy-benzamide (MIP-1145), was evaluated for its ability to distinguish melanin-expressing from amelanotic human melanoma cells, and to localize specifically to melanin containing tumor xenografts. The binding of [¹³¹I]MIP-1145 to melanoma cells *in vitro* was melanin-dependent, increased over time, and insensitive to mild acid treatment, indicating that it was retained within cells. Cold carrier MIP-1145 did not reduce the binding, consistent with the high capacity of melanin binding of benzamides. In human melanoma xenografts, [¹³¹I]MIP-1145 exhibited diffuse tissue distribution and washout from all tissues except melanin expressing tumors. Tumor uptake of 8.82% injected dose per gram (ID/g) was seen at 4 hours post-injection and remained at 5.91% ID/g at 24 hours, with tumor:blood ratios of 25.2 and 197, respectively. Single photon emission computed tomography (SPECT) imaging was consistent with the tissue distribution results. The administration of [¹³¹I]MIP-1145 at 25 MBq or 2.5 GBq/m² in single or multiple doses significantly reduced SK-MEL-3 tumor growth with multiple doses resulting in tumor regression and a durable response for over 125 days. To estimate human dosimetry, gamma camera imaging and pharmacokinetic analysis was performed in cynomolgus monkeys. The melanin-specific binding of [¹³¹I]MIP-1145, combined with prolonged tumor retention, the ability to significantly inhibit tumor growth, and acceptable projected human dosimetry, suggest that it may be effective as a radiotherapeutic pharmaceutical for treating patients with metastatic malignant melanoma.

Introduction

The incidence of malignant melanoma is rising faster than that of any other cancer in the United States, and The Skin Cancer Foundation estimates that approximately 60,000 new cases will be diagnosed this year. Unfortunately, the prognosis for stage 3 and 4 disease is poor. Currently,

Author to whom correspondence and reprint requests should be addressed: John W. Babich, Ph.D., 160 Second Street, Cambridge, MA 02142, USA, Tel: (617) 492-5554, FAX: (617) 871-6980, jbabich@molecularinsight.com.

Disclosure of potential conflicts of interest: This work was conducted at Molecular Insight Pharmaceuticals, Inc. J. Joyal, J. Barrett, J. Marquis, J. Chen, S. Hillier, K. Maresca, J. Kronauge and J. Babich are employees of Molecular Insight Pharmaceuticals, Inc. R. Mairs and M. Pomper are consultants for Molecular Insight Pharmaceuticals, Inc.

there is no effective treatment for melanoma metastases, and patients with metastatic disease have a life expectancy of 4-6 months. Complete surgical removal of the diseased tissue is commonly used to treat the primary tumor. However, due to early and wide-spread occurrence of metastases as small as 3 mm in diameter, surgery is often not curative, and chemotherapeutic options are limited with poor response rates. Current FDA-approved treatments for stage 4 melanoma include Dacarbazine with an objective response rate of 16% (1), and high-dose bolus IL-2 (Proleukin™) also with an objective response rate of 16% (2). High-dose interferon alpha-2b (Intron™ A) is approved for high-risk stage 2 and 3 melanoma and has an objective response rate of 14% in stage 4 disease (3). The combination of IL-2 and interferon alpha occasionally produces relatively long durations of response, but do not benefit enough patients to improve median survival substantially; in addition, these agents are associated with significant toxicity (4-7). The poor response rates with these regimens suggest a large unmet need for effective treatments for patients with metastatic melanoma.

The vast majority of melanomas contain the pigment melanin (8), which is produced within cells during the metabolism of tyrosine. Melanin is found in all pigmented regions of the body including the skin, hair and eyes, and is also found in the inner ear and in regions of the brain, specifically within the substantia nigra (9,10). Melanins are biopolymers containing indole units with carboxyl functionalities and phenolic hydroxy groups (11), which appear to have multiple homeostatic and protective functions. In the skin, melanin protects against the harmful effects of ultraviolet radiation, and melanogenesis is stimulated by DNA damage caused by ultraviolet rays. In addition, melanin plays a role in absorbing heat. Importantly, organic amines, metals, and polycyclic aromatic hydrocarbons are capable of binding melanin in normal and malignant tissues (12). Drug-melanin associations involve a complex array of hydrogen bonding, hydrophobic and ionic interactions, and both cooperative and anti-cooperative binding (13,14). However, those interactions have not been fully characterized, partly because melanins are not well-defined chemical entities but rather are mixtures of polymers with non-hydrolyzable bonds. The physiological significance of compound-binding to normal melanotic tissue is not clear. While it may lead to the removal of harmful substances from the body (15), it could potentially have detrimental effects as it sequesters toxic or carcinogenic chemicals (9,12,14).

Radiolabeled benzamide derivatives are known to bind melanin, and exhibit high uptake and retention in melanoma cells and in mice bearing melanoma tumors (16-21), making them potentially effective agents for detecting melanoma in patients and for delivery of therapeutic isotopes. For the last 20 years efforts have focused on the development of melanin-localizing benzamides that exhibit rapid washout from non-target tissues and prolonged tumor retention for the treatment of metastatic melanoma. Here we describe the preclinical evaluation of *N*-(2-diethylamino-ethyl)-4-(4-fluoro-benzamido)-5-iodo-2-methoxy-benzamide (MIP-1145), an ¹³¹I-labeled small molecule benzamide that may be effective for therapeutic targeting of melanin-positive melanoma.

Methods

Radiolabeling of [¹³¹I]MIP-1145 and [¹²³I]MIP-1145

N-(2-diethylamino-ethyl)-4-(4-fluorobenzamido)-2-methoxy-benzamide (MIP-1145 precursor, 80 ug) dissolved in acetic acid, was added to thallium trifluoroacetate, Tl(TFA)₃ in trifluoroacetic acid (TFA) in a molar ratio of 1-1.2. The solution was brought to a final volume of 0.3 mL (50% acetic acid, 50% TFA). After a 10 minute incubation at room temperature, 2.2 GBq of Na¹³¹I (or Na¹²³I for SPECT/CT) in 10-20 uL of 0.1 N NaOH was added and incubated at room temperature for an additional 5 minutes. The crude reaction was diluted in formulation buffer (6% PEG-400, 2% ethanol, 6% ascorbic acid, and 3% sodium gentisate, pH 4.4) then purified/analyzed on a Zorbax Eclipse Plus C18, 4.6 × 100 mm, 5 um reversed phase high

performance liquid chromatography (RP-HPLC) column. The column was eluted with a gradient of 25-60% buffer B over 10 minutes at a flow rate of 2 mL/min using 2.5% ascorbic acid (w/v)/0.5% acetic acid (v/v) in water (buffer A) and 2.5% ascorbic acid (w/v)/85% ethanol (v/v) in water (buffer B) as the solvents. The product peak was collected and diluted in formulation buffer to a final concentration of 1.48 MBq/mL. The solution was filtered through a sterile Millipore Millex GV 33mm, 0.2 μ m syringe filter to yield the final product with a radiochemical purity (RCP) of >95 % and a specific activity as high as 55.5 TBq/mmol.

Cell Culture

The human melanoma cell line, SK-MEL-3, and the human amelanotic melanoma cell line, A375, were obtained from the American Type Culture Collection. A375 cells were maintained in Dulbecco's Modified Eagles Medium (D-MEM) (Invitrogen) supplemented with 10% fetal bovine serum (FBS) (Hyclone). SK-MEL-3 cells were maintained in McCoy's 5a (modified) medium (Invitrogen) containing 15% FBS. All cells were grown in a humidified incubator at 37 °C/5% CO₂. Cells were passaged by washing in Dulbecco's Phosphate Buffered Saline (D-PBS) (Invitrogen) and incubating them at 37°C with 0.25% trypsin/EDTA (Invitrogen).

Binding of [¹³¹I]MIP-1145 to Cells

Cells were plated in Costar 96-well culture plates (50,000 cells per well for SK-MEL-3 cells and 25,000 cells per well for A375 cells) and allowed to attach overnight. Due to differences in growth rate, plating cells at these densities resulted in both cell lines reaching confluence by the following morning, allowing for a straightforward comparison. To examine the time course of [¹³¹I]MIP-1145 uptake, cells were incubated for various times up to 6 hours with 11.5 nM [¹³¹I]MIP-1145 (approximately 9×10^5 CPM/well) in D-MEM containing 0.5% bovine serum albumin (BSA). At the indicated time, the medium was removed and the cells were washed once with D-MEM/0.5% BSA. The cells were then washed with a mild acid buffer (50 mM glycine, 150 mM NaCl, pH 3.0) at 4 °C for 5 minutes. The buffer was collected and the cells were washed once with D-MEM/0.5% BSA. Pooled washes (containing cell surface bound [¹³¹I]MIP-1145) were counted on a Wallac 1282 automated gamma counter. The culture plate (containing cells with internalized [¹³¹I]MIP-1145) was counted on a Wallac 1450 Trilux Microbeta liquid scintillation counter. Counts on both instruments were calibrated to a standard. For competitive binding analysis, cells were incubated for 2 hours with 3.6 nM [¹³¹I]MIP-1145 in the presence of 1.6-1,600 nM non-radiolabeled MIP-1145. All plates were washed twice with D-MEM/0.5% BSA containing 50 mM HEPES buffer, 150 μ L of scintillation fluid was added per well, and plates were counted on a liquid scintillation counter.

Tissue Distribution of [¹³¹I]MIP-1145

Male athymic NCr^{nu/nu} mice (Taconic) were anesthetized by an intraperitoneal injection of 9.5 mg/mouse avertin. SK-MEL-3 cells and A375 cells were resuspended at 8×10^6 cells/mL in a 1:1 mixture of D-PBS containing 1 g/L D-glucose and 36 mg/L L-sodium pyruvate (Invitrogen) and Matrigel (BD Biosciences). Each mouse was injected in the right hind flank with 0.25 mL of the cell suspension. Mice were used for tissue distribution studies when the tumors reached 100-500 mm³ (approximately 21 days post-inoculation).

A quantitative analysis of the tissue distribution of [¹³¹I]MIP-1145 was performed in separate groups of male NCr^{nu/nu} mice bearing SK-MEL-3 or A375 xenografts. [¹³¹I]MIP-1145 was administered via the tail vein as a bolus injection of approximately 74 KBq in a constant volume of 0.05 mL. Mice (n=5/time point) were euthanized by asphyxiation with carbon dioxide at 1, 4 and 24 hours post-injection. Tissues (blood, heart, lungs, liver, spleen, kidneys, stomach (with contents), large and small intestines (with contents), testes, skeletal muscle, bone, brain, adipose and tumor) were dissected, excised, weighed wet, transferred to plastic tubes and counted in an automated gamma counter.

SPECT Imaging

Athymic nude mice were implanted with 5×10^6 SK-MEL-3 or A375 cells. When the tumors reached 100-500 mm³, mice were anesthetized using 1% isoflurane gas in oxygen flowing at 0.6 L/min prior to and during radiopharmaceutical injection. Mice were injected via the tail vein with 37 MBq [¹²³I]MIP-1145 and imaged at 1, 4 and 24 hours post-injection with a Gamma Medica X-SPECT scanner equipped with two medium energy collimators with a radius-of-rotation of 9 cm. The tomographic data were acquired in 64 projections over 360 degrees at 40 seconds/projection. Following tomography, CT imaging was acquired in 512 projections to allow anatomic co-registration. Data were reconstructed using the ordered subsets-expectation maximization algorithm (2D OS-EM). Maximum intensity projection images were generated using Amira 5.2.0 software (Visage Imaging).

Effect of [¹³¹I]MIP-1145 on SK-MEL-3 Growth

Six week old female athymic nude mice (Charles River Laboratories) were inoculated subcutaneously with human melanoma SK-MEL-3 cells (3×10^6 cells) into the right hind flank. When tumors reached an average volume of ~100 mm³, animals were randomly assigned to one of the treatment groups (n = 10 mice per group) which included: saline, [¹³¹I]MIP-1145 at 25 MBq or 2.5 GBq/m² single dose, [¹³¹I]MIP-1145 once weekly for 2 weeks, and [¹³¹I]MIP-1145 once weekly for 3 weeks. Each animal was administered the test article intraperitoneally in a volume of 0.1 mL. Tumor dimensions were measured twice weekly with digital calipers and tumor volumes were calculated with the formula (width² × length)/2. Mice were followed until tumor volumes in the vehicle group reached the maximum allowed by IACUC guidelines (1,500 mm³). To monitor potential toxicity, body weight was measured daily and animals were scored for signs of distress using standard guidelines (22).

Dosimetry in Cynomolgus Monkeys

Four cynomolgus monkeys (2 female and 2 male) anesthetized with Telazol received an intravenous dose of 185 MBq [¹³¹I]MIP-1145 without thyroid blockade. Serial anterior/posterior imaging was performed on a Siemens dual head E-cam gamma camera. The duration of acquisition was adjusted to achieve adequate organ count density. Blood sampling was performed at 5, 30, 60, 120, 360 minutes and at 24, 48 and 72 hours post-injection. Urine was collected from all animals through the 72 hour time point at the following collection intervals: 0-6 hours, 6-24 hours, 24-48 hours and 48-72 hours post-injection.

The pharmacokinetics of [¹³¹I]MIP-1145 was analyzed by WinNonlin 4.1 (Pharsight). The blood and tissue concentration-time data were computed by a non-compartment method and pharmacokinetic parameters (maximum concentration, C_{max}; area-under-curve, AUC; mean residence time, MRT) were generated. Total clearance (CL) was calculated as CL=dose/AUC, and steady-state volume of distribution (V_{ss}) was calculated as V_{ss}=MRT*CL using model 201. Regions of interest were drawn on the anterior and posterior images over the animal's total body, lung, kidney, thyroid, and eye regions at each time point (where these regions were visible). Total organ uptake was normalized to a percentage of the total body dose where the amount of retention at the first image (prior to voiding) was 100%. Time integrals of whole body and target organ retention were entered into OLINDA/EXM software (23). The adult male human phantom model was used with a 4.8 hour voiding interval for the urinary bladder. The OLINDA/EXM unit density sphere model was used to estimate average dose to the eye.

Results

Radiolabeling of [¹³¹I]MIP-1145

The structure of MIP-1145 is shown in Figure 1. MIP-1145 was readily radiolabeled with ¹³¹I or ¹²³I *via* Tl(TFA)₃, starting with the precursor, *N*-(2-diethylamino-ethyl)-4-(4-fluorobenzamido)-2-methoxy-benzamide. The crude reaction solution was purified by RP-HPLC and the product was collected in radiolysis stabilizing media (6% ascorbic acid, and 3% sodium gentisate, pH 4.5). Typically, a radiochemical yield of 70-90% with a RCP of greater than 95% for the final product was obtained. [¹³¹I]MIP-1145 was stable in both saline and rat plasma (>94%) at 37 °C for at least 24 hours.

[¹³¹I]MIP-1145 Binds Specifically to Melanotic Cells and is Internalized

To examine binding of [¹³¹I]MIP-1145 to melanotic SK-MEL-3 cells and amelanotic A375 cells, confluent cultures were incubated with [¹³¹I]MIP-1145 for various times up to 6 hours, and washed with either medium or a mild acid solution to remove compound that is bound to the cell surface. Figure 2A depicts the total binding of [¹³¹I]MIP-1145 and the acid insensitive binding or internalized compound in SK-MEL-3 and A375 cells. Total binding was approximately twice as great for the SK-MEL-3 cells compared to the A375 cells. These results show a time dependent, acid insensitive increase in radioactivity associated with the cellular pellet of SK-MEL-3, but not with A375 cells. After 6 hours, approximately 43% of the total MIP-1145 added to the SK-MEL-3 cells was cell associated, whereas only about 13% of MIP-1145 was associated with A375 cells, indicating that MIP-1145 is preferentially retained within the melanin expressing SK-MEL-3 cells. A competitive binding assay was performed to evaluate the ability of non-radiolabeled MIP-1145 to compete with [¹³¹I]MIP-1145 for binding to melanin in SK-MEL-3 and A375 cells. As shown in Figure 2B, [¹³¹I]MIP-1145 bound to a much greater extent to SK-MEL-3 cells compared to A375 cells. Importantly, there was very little competition by non-radiolabeled MIP-1145 for binding, up to the maximum concentration tested of 1.6 μM. These data suggest a high capacity binding of MIP-1145 to melanin such that high specific radioactivity is not necessary for effective melanoma uptake.

[¹³¹I]MIP-1145 Localizes to Melanotic Tissues

The tissue distribution of [¹³¹I]MIP-1145 was assessed in NCr^{nu/nu} mice bearing SK-MEL-3 or A375 xenografts (Table I). At 1 hour, [¹³¹I]MIP-1145 exhibited diffuse tissue distribution with the greatest uptake in the kidneys, gastrointestinal tract and liver, demonstrating that [¹³¹I]MIP-1145 clears *via* both renal and hepatobiliary routes. By 4 hours, all non-target and non-excretory tissues had begun to clear, while uptake in the SK-MEL-3 tumors, but not the A375 tumors, had increased. SK-MEL-3 tumor uptake of 8.82 %ID/g was detected at 4 hours post-injection and remained at 5.91 %ID/g at 24 hours, with tumor:blood ratios of 25.2 and 197, respectively. Minimal deiodination was observed as the thyroid contained <1% of the total injected dose at all time points. High uptake was noted in the stomach. Although this is unusual, it has been observed with compounds of this class (24). While we have reported high uptake of [¹³¹I]MIP-1145 in the pigmented eyes of C57BL6 mice (>30% ID/g) (25), as expected, there was very little uptake (<1% ID/g) in the unpigmented eyes of the albino NCr^{nu/nu} mice.

SPECT/CT imaging with [¹²³I]MIP-1145 was consistent with the tissue distribution results (Figure 3). SK-MEL-3 tumors were easily discernible at all time points examined, while A375 tumors were not detected. At 1 hour post-injection, diffuse tissue distribution was observed with the greatest uptake in the tumor, kidneys, gastrointestinal tract and liver. By 24 hours, tumor uptake was still visualized, along with only remnants of [¹²³I]MIP-1145 detected in the lower gastrointestinal tract.

[¹³¹I]MIP-1145 Inhibits the Growth of Melanotic Xenograft Tumors and Prolongs Survival

To determine if [¹³¹I]MIP-1145 has the potential to be used as a radiotherapeutic drug, the effect of [¹³¹I]MIP-1145 treatment on tumor growth was examined (Figure 4A). Twenty one days after implantation, SK-MEL-3 tumors reached a volume of $123 \pm 8 \text{ mm}^3$ and animals were randomly assigned to one of the four treatment groups. Saline treatment resulted in a linear growth rate over the first 60 days of the study. During this time the tumor size increased more than 10-fold for a tumor doubling time of approximately 3 days. Several animals in the saline group either died with tumor or had to be sacrificed when the tumor reached the maximum allowed size by IACUC guidelines, $1,500 \text{ mm}^3$. A single dose of [¹³¹I]MIP-1145 at 25 MBq or 2.5 GBq/m² resulted in a marked reduction in the rate of tumor growth. At 35 days after a single treatment the average tumor volume was only 2.2 times greater than the starting volume resulting in a reduction in tumor volume of approximately 79% compared to saline. Two doses of [¹³¹I]MIP-1145 administered one week apart resulted in tumor regression of 11% at 35 days compared to the starting volume. Three doses of [¹³¹I]MIP-1145 administered one week apart resulted in a further tumor reduction at 35 days of 40% compared to the starting volume. At 120 days post administration of the first dose of [¹³¹I]MIP-1145, inhibition of tumor growth was still obvious in all treatment groups, with the group that received three doses of [¹³¹I]MIP-1145 exhibiting no significant tumor growth compared to the initial pre-treatment starting volume. [¹³¹I]MIP-1145 treatment resulted in a dose dependent increase in survival. By day 120, 90% of the animals in the saline group either died with tumor or had to be sacrificed (Figure 4B). In contrast, 60% of the one dose [¹³¹I]MIP-1145 group, 90% of the two dose [¹³¹I]MIP-1145 group, and 100% of the three dose [¹³¹I]MIP-1145 group survived the 120 day course of the experiment. No significant changes in body weight or signs of distress were observed with [¹³¹I]MIP-1145 treatment indicating minimal toxicity.

Dosimetry of [¹³¹I]MIP-1145 Suggests Potential Use as a Therapeutic in Humans

To examine dosimetry, gamma camera imaging and pharmacokinetic analysis was performed on cynomolgus monkeys injected with 185 MBq [¹³¹I]MIP-1145. After reaching C_{max} at the first time point, the blood concentration slowly declined with a MRT of 47 ± 5 hours. Mean blood clearance was $400 \pm 45 \text{ mL/hour}$ indicating that [¹³¹I]MIP-1145 was slowly cleared from the vascular compartment with a V_{ss} of $19 \pm 3.1 \text{ L}$. This value is greater than the total body water of the cynomolgus monkey indicating that [¹³¹I]MIP-1145 was highly distributed outside the vascular compartment. Although this study was not designed to be a mass balance analysis, by 72 hours post-injection, 28% of the injected dose was recovered in the urine. Scintigraphic images showed that [¹³¹I]MIP-1145 was slowly cleared predominantly via the hepatobiliary route as evidenced by uptake in the gall bladder and gastrointestinal tract. Ocular retention was observed beginning 24-48 hours post-injection. Uptake in the thyroid was also visualized beginning at 24 hours post-injection as expected since thyroid blockade was not conducted.

Radiation dose estimates of [¹³¹I]MIP-1145 for human organs were extrapolated from the cynomolgus monkey scintigraphic distribution data. The results of this analysis showed the target organs to be the thyroid, large intestine and eyes, which received radiation absorbed doses of 18, 2.8/1.1 (lower/upper), and 1.3 mGy/MBq, respectively. All other organs were predicted to receive between 0.064-1.1 mGy/MBq (Table II).

Discussion

The value of radiolabeled benzamides for imaging melanoma *via* affinity for melanin was first realized in 1986 when iodine-labeled compounds under investigation for brain imaging were shown to localize to the pigmented eyes of C57BL6 mice but not the unpigmented eyes of Wistar albino rats (26). It was later determined that uveal melanin mediated the uptake (26). Since these initial observations, several ¹²³I-labeled molecules have been examined for

scintigraphic detection of malignant melanoma in patients *via* melanin content (16,17,27). *N*-(2-diethylamino-ethyl 4-iodobenzamide) (BZA), the first molecule to advance to clinical trials, demonstrated a sensitivity of 81% and a specificity of 100% on a lesion site basis in patients with confirmed melanoma, thereby validating the concept (28).

More recently, several laboratories have focused on the development of benzamide analogs incorporating ^{131}I for radiotherapy (18). Na^{131}I is commonly used to treat thyroid cancer as it emits a high energy (606 keV) β particle capable of ablating the cancer and its metastases. For consideration for radiotherapy, compounds must exhibit significant uptake and prolonged tumor retention and rapid washout from non-target tissues. [^{131}I]MIP-1145 was selected as a lead from a series of ring substituted benzamides based on the level of tumor uptake *in vivo*, chemical stability and aqueous solubility (25). MIP-1145 retains a similar pharmacophore to BZA and other melanin-binding benzamides, but is modified to include a methoxy group at the 2-position and an iodine at the 5-position of the central aromatic ring, which was used here for radiolabeling with ^{131}I and ^{123}I in high radiochemical yield and purity. In addition, MIP-1145 contains a fluorobenzoate, which could potentially be radiolabeled with ^{18}F for monitoring the success of radiotherapy by positron emission tomography (PET).

MIP-1145 exhibited melanin-specific binding, washout from non-target tissues and prolonged tumor retention, making it an ideal candidate for systemic radiotherapy. The high uptake of MIP-1145 is in agreement with observations made using other radiolabeled benzamides (16-21), and is consistent with the binding properties of the melanin polymer, which unlike a typical receptor-ligand interaction, involves multiple types of associations resulting in the sequestration of large amounts of material in essentially a non-specific, non-competitive fashion (19). Similarly, tumor uptake in mice bearing B16F10 xenografts was unchanged by lowering the specific activity of the [^{131}I]MIP-1145 by 1,000-fold from 55.5 TBq/mmol to 55.5 GBq/mmol, 10.17 ± 1.81 vs. 9.28 ± 2.24 %ID/g, respectively (25).

Treatment of mice bearing melanin-containing SK-MEL-3 tumors with a single dose of [^{131}I]MIP-1145 resulted in a dramatic inhibition of tumor growth, with significant tumor regression at multiple doses. These tumor growth inhibition data with [^{131}I]MIP-1145 are notable as there are presently very few effective treatment options for patients with advanced metastatic melanoma. Future dose optimization studies in humans are necessary to select a regimen that is efficacious while delivering the lowest amount of radiation possible to normal tissues to avoid potential toxicity.

As expected, there was very little uptake of [^{131}I]MIP-1145 in the unpigmented eyes of albino $\text{NCR}^{nu/nu}$ mice. However, we previously reported high uptake of [^{131}I]MIP-1145 in the pigmented eyes of C57BL6 mice (>30% ID/g) (25). Therefore, it was essential to forecast the exposure to the eyes of melanoma patients. Using a Monte Carlo simulation, the radiation dose estimates to the human eye were obtained from monkey scintigraphic data for ^{131}I accumulated in three melanin-containing substructures (ciliary body, retina, and choroid). The ocular substructure simulation predicted a radiation absorbed dose of 0.2 MBq-hr/MBq, with the highest radiation absorbed dose to the ciliary body (6.8 Gy for a 3.7 GBq therapeutic dose). Using the results from external beam data, the $\text{TD}_{5/5}$ (5% incidence in 5 years) values for retinopathy and cataract induction are 45 Gy and 10 Gy, respectively (29). Therefore, an administered activity of 20.8 GBq would be needed to reach the retina $\text{TD}_{5/5}$ of 45 Gy for retinopathy, and an administered activity of 7.7 GBq would be needed to reach the lens $\text{TD}_{5/5}$ of 10 Gy for cataracts. Estimates of the human radiation dose for [^{131}I]MIP-1145, based on an extrapolation of non-human primate scintigraphy and dosimetry calculations, support the safe administration of therapeutic doses of up to 16.2 GBq with the anticipated dose-limiting organ being the lower large intestine. Based on the mouse xenograft results, the anticipated efficacious human dose will be 2.5 GBq/m² or 4.7 GBq/70 kg patient. At this dose the radiation

absorbed dose to the lower large intestine will be 13.3 Gy which is 3.3 times less than the allowable radiation exposure limit of 45 Gy, and the dose to the eye is only 6.1 Gy. Based on this profile we anticipate a sufficient therapeutic index to warrant the study of [¹³¹I]MIP-1145 in the treatment of Stage 3 and Stage 4 melanoma. It also may be advantageous to combine [¹³¹I]MIP-1145 with chemotherapeutic drugs or radiation sensitizing agents, as has been done in animal models with [¹³¹I]-meta-iodobenzylguanidine, to enhance efficacy at low doses of radiation (30-33).

While normal melanosomes have a protective function by virtue of their detoxification of reactive oxygen species (ROS), these organelles in melanoma cells are deviant inasmuch as they generate free radicals (34,35). This may be a result of metal binding to the characteristic pigment structure (36), or a consequence of melanin biosynthesis (37). Chronic production of oxidative stress could contribute to the malignant transformation process (38). Conversely, the melanoma-specific accumulation of ROS may provide a unique therapeutic target (38), and recent evidence indicates that the ROS-inducing drug Elesclomol potentiates apoptosis in melanoma cells through the induction of oxidative stress (39). The sensitivity of melanoma cells to therapeutic schemes that promote cell death through ROS production encourages the use of ionizing radiation combined with the specificity afforded by melanoma-selective targeting using melanin avid small molecules.

Radiation therapy has not commonly been employed to treat melanoma because melanoma cells in culture have traditionally been considered radiation resistant (40). Rofstad, in assessing the effect of radiation on several human melanoma cell lines, concluded that malignant melanoma is heterogeneous in radio-responsiveness, and therefore malignant melanomas should not be considered radiation resistant in general (41,42). Recently, several clinical studies have realized success using external beam radiation as a means of palliation in patients with metastatic melanoma (43,44), dispelling the concept that melanoma is radiation resistant. While focused external radiation may be effective for local control, its use to treat widespread disease is obviously limited. In addition, intense local irradiation can result in significant undesirable damage to adjacent, normal tissues. Targeted radiotherapy, as exemplified here with [¹³¹I]MIP-1145, offers the advantage of directing the radioactive payload specifically to tumor cells *via* binding to a cancer-associated molecular target, thereby sparing non-target tissues. This should be especially beneficial for patients with widespread metastases where conventional radiotherapy is not applicable.

Interestingly, moderate uptake of [¹³¹I]MIP-1145 was detected in the mouse brain, reaching approximately 0.6-0.8 %ID/g, indicating that [¹³¹I]MIP-1145 crosses the blood-brain barrier. Blood-brain barrier permeability is critical for treating melanoma metastases to the brain. This is particularly encouraging given that the presence of brain metastases confers a poor prognosis, and two-thirds of melanoma patients die with brain metastases (45).

Alternative strategies to exploit melanin, melanogenesis and the interaction of benzamides with melanin for the potential treatment of melanoma have met with early but in some cases limited success. In this regard, alkylating benzamides have been shown to promote tumor growth delay in preclinical models (46), and high tumor uptake has been observed with radiolabeled acridine conjugated benzamides (47). Radiolabeled analogs of α-MSH peptide have also shown some promise in animal models (48). Furthermore, radiolabeled anti-melanin antibodies for imaging and treatment of melanoma have demonstrated efficacy in preclinical models (49,50). However, as melanin is intracellular, antibodies are only expected to bind to necrotic tumor cells. In addition, the long circulating half-life of antibodies results in enhanced non-target tissue exposure, often limiting the dose that can be administered. Thus, small molecule benzamides, like [¹³¹I]MIP-1145, which freely traverse the cell membrane to reach the

intracellular target and clear rapidly from the circulation and non-target tissues, offer a more effective approach.

In summary, described here is a new radiolabeled benzamide analog, [¹³¹I]MIP-1145, which as a result of its localization to melanin expressing tumors, exhibits efficacy in inhibiting melanoma growth *in vivo*. In light of the large unmet medical need, these data strongly support the advancement of [¹³¹I]MIP-1145 to clinical trials for further evaluation as a radiotherapeutic pharmaceutical for treating patients with malignant melanoma.

Acknowledgments

The US National Institute of Health and National Cancer Institute are graciously acknowledged for financial support of grant R44 CA 138041 and U24 CA 92871.

References

1. Eggermont AM, Kirkwood JM. Re-evaluating the role of dacarbazine in metastatic melanoma: what have we learned in 30 years? *Eur J Cancer* 2004;40:1825–36. [PubMed: 15288283]
2. Atkins MB, Lotze MT, Dutcher JP, et al. High-dose recombinant interleukin 2 therapy for patients with metastatic melanoma: analysis of 270 patients treated between 1985 and 1993. *J Clin Oncol* 1999;17:2105–16. [PubMed: 10561265]
3. Sertoli MR, Bernengo MG, Ardizzoni A, et al. Phase II trial of recombinant alpha-2b interferon in the treatment of metastatic skin melanoma. *Oncology* 1989;46:96–8. [PubMed: 2710482]
4. Atallah E, Flaherty L. Treatment of metastatic malignant melanoma. *Curr Treat Option On* 2005;6:185–93.
5. Tarhini AA, Agarwala SS. Cutaneous melanoma: available therapy for metastatic disease. *Dermatol Ther* 2006;19:19–25. [PubMed: 16405566]
6. Tarhini AA, Agarwala SS. Interleukin-2 for the treatment of melanoma. *Curr Opin Inv Drug* 2005;6:1234–9.
7. Tarhini AA, Agarwala SS. Novel agents in development for the treatment of melanoma. *Expert Opin Inv Drug* 2005;14:885–92.
8. Gualandri L, Betti R, Crosti C. Clinical features of 36 cases of amelanotic melanomas and considerations about the relationship between histologic subtypes and diagnostic delay. *J Eur Acad Dermatol* 2009;23:283–7.
9. Tolleson WH. Human melanocyte biology, toxicology, and pathology. *J Environ Sci Health C* 2005;23:105–61.
10. Sulaimon SS, Kitchell BE. The biology of melanocytes. *Vet Dermatol* 2003;14:57–65.
11. Prota G. Melanins, melanogenesis and melanocytes: looking at their functional significance from the chemist's viewpoint. *Pigm Cell Res* 2000;13:283–293.
12. Larson BS. Interaction between chemicals and melanin. *Pigm Cell Res* 1993;6:127–33.
13. Knorle R, Schniz E, Feuerstein TJ. Drug accumulation in melanin: an affinity chromatography study. *J Chromatogr B Biome Sci Appl* 1998;714:171–9.
14. Birdelli MG, Ciati A, Crippa PR. Binding of chemicals to melanins re-examined: Adsorption of some drugs to the surface of melanin particles. *Biophys Chem* 2006;119:137–45. [PubMed: 16139945]
15. Land, EJ.; Ramsden, CA.; Riley, PA. Toxicological aspects of melanin and melanogenesis. In: Nordlund, JJ.; Boissy, RE.; Hearing, VJ.; King, RA.; Oetting, WS.; Ortonne, J., editors. *The pigmentary system: physiology and pathophysiology*. 2nd. Blackwell Publishing Ltd; 2006.
16. Brandau W, Niehoff T, Pulawski P, et al. Structure distribution relationship of iodine-123-iodobenzamides as tracers for the detection of melanotic melanoma. *J Nucl Med* 1996;37:1865–71. [PubMed: 8917194]
17. Larisch R, Schulte K, Vosberg H, et al. Differential accumulation of iodine-123-iodobenzamide in melanotic and amelanotic melanoma metastases *in vivo*. *J Nucl Med* 1998;39:996–1001. [PubMed: 9627332]

18. Eisenhut M, Hull WE, Mohammed A, et al. Radioiodinated N-(2-diethylaminoethyl)benzamide derivatives with high melanoma uptake: Structure-affinity relationships, metabolic fate, and intracellular localization. *J Med Chem* 2000;43:3913–22. [PubMed: 11052796]
19. Labarre P, Papon J, Moreau MF, et al. Melanin affinity of N-(2-diethylaminoethyl)-4-iodobenzamide, an effective melanoma imaging agent. *Melanoma Res* 2002;12:115–21. [PubMed: 11930107]
20. Mansard S, Papon J, Moreau MF, et al. Uptake in melanoma cells of N-(2-diethylaminoethyl)-2-iodobenzamide (BZA2), an imaging agent for melanoma staging: relation to pigmentation. *Nucl Med Biol* 2005;32:451–8. [PubMed: 15982575]
21. Pham TQ, Greguric I, Liu X, et al. Synthesis and evaluation of novel radioiodinated benzamides for malignant melanoma. *J Med Chem* 2007;50:3561–72. [PubMed: 17602544]
22. Morton DB, Griffiths PHM. Endpoints in animal study protocols. *Vet Record* 1985;116:43143.
23. Stabin MG, Sparks RB, Crowe E. OLINDA/EXM: The second-generation personal computer software for internal dose assessment in nuclear medicine. *J Nucl Med* 2005;46:1023–7. [PubMed: 15937315]
24. Bonnet-Duquennoy M, Papon J, Mishellany F, et al. Promising pre-clinical validation of targeted radionuclide therapy using a [¹³¹I] labeled iodoquinoline derivative for an effective melanoma treatment. *J Canc Sci Ther* 2009;1:1–7.
25. Joyal JL, Hillier SM, Marquis JC, et al. Molecular targeting of melanoma with radiolabeled benzamides. *J Nucl Med* 2008;49(Suppl 1):16P.
26. Michelot JM, Moreau MFC, Labarre PG, et al. Synthesis and evaluation of new iodine-125 radiopharmaceuticals as potential tracers for malignant melanoma. *J Nucl Med* 1991;32:1573–80. [PubMed: 1869982]
27. Nicholl C, Mohammed A, Hull WE, Bubeck B, Eisenhut M. Pharmacokinetics of iodine-123-IMBA for melanoma imaging. *J Nucl Med* 1997;38:127–33. [PubMed: 8998166]
28. Michelot JM, Moreau MFC, Veyre AJ, et al. Phase II scintigraphic clinical trial of malignant melanoma and metastases with iodine-123-N(2-diethylaminoethyl 4-iodobenzamide). *J Nucl Med* 1993;34:1260–6. [PubMed: 8326382]
29. Emami B, Lyman J, Brown A, et al. Tolerance of normal tissue to therapeutic irradiation. *Int J Rad Oncol Biol Phys* 1991;21:109–22.
30. McCluskey AG, Boyd M, Gaze MN, Mairs RJ. [¹³¹I]MIBG and topotecan: a rationale for combination therapy for neuroblastoma. *Cancer Letters* 2005;228:221–7. [PubMed: 15935554]
31. McCluskey AG, Boyd M, Ross SC, et al. [¹³¹I]meta-iodobenzylguanidine and topotecan combination treatment of tumours expressing the noradrenaline transporter. *Clin Cancer Res* 2005;11:7929–37. [PubMed: 16278418]
32. Gaze MN, Chang YC, Flux GD, Mairs RJ, Saran FH, Meller ST. Feasibility of dosimetry-based high-dose ¹³¹I-meta-iodobenzylguanidine with topotecan as a radiosensitizer in children with metastatic neuroblastoma. *Cancer Biother Radio* 2005;20:195–9.
33. Mairs RJ, Boyd M. Optimizing MIBG therapy of NETs - preclinical evidence of dose maximization and synergy. *Nucl Med Biol* 2008;35:S9–20. [PubMed: 18707637]
34. Gidanian S, Mentelle M, Meyskens FL, Farmer PJ. Melanosomal damage in normal human melanocytes induced by UVB and metal uptake—A basis for the pro-oxidant state of melanoma. *Photochem Photobiol* 2008;84:556–64. [PubMed: 18331399]
35. Wittgen HG, van Kempen LC. Reactive oxygen species in melanoma and its therapeutic implications. *Melanoma Res* 2007;17:400–9. [PubMed: 17992124]
36. Smit NP, van Nieuwpoort FA, Marrot L, et al. Increased melanogenesis is a risk factor for oxidative DNA damage—study on cultured melanocytes and atypical nevus cells. *Photochem Photobiol* 2008;84:550–5. [PubMed: 18435613]
37. Fruehauf JP, Trapp V. Reactive oxygen species: an Achilles' heel of melanoma? *Expert Rev Anticanc* 2008;8:1751–7.
38. Fruehauf JP, Meyskens FL. Reactive oxygen species: A breath of life or death? *Clin Cancer Res* 2007;13:789–94. [PubMed: 17289868]
39. Kirshner JR, He S, Balasubramanyam V, et al. Elesclomol induces cancer cell apoptosis through oxidative stress. *Mol Cancer Ther* 2008;7:2319–27. [PubMed: 18723479]

40. Barranco SC, Romsdahl MM, Humphrey RM. The radiation response of human malignant melanoma cells grown in vitro. *Cancer Res* 1971;31:830–3. [PubMed: 5088486]
41. Einar R. Radiation sensitivity in vitro of primary tumors and metastatic lesions of malignant melanoma. *Cancer Res* 1992;52:4453–7. [PubMed: 1643637]
42. Rofstad EK. Radiation biology of malignant melanoma. *Acta Radiol Oncol* 1986;25:1–10. [PubMed: 3010642]
43. Olivier KR, Schild SE, Morris CG, Brown PD, Markovic SN. A higher radiotherapy dose is associated with more durable palliation and longer survival in patients with metastatic melanoma. *Cancer* 2007;110:1791–5. [PubMed: 17721993]
44. Berk LB. Radiation therapy as primary and adjuvant treatment for local and regional melanoma. *Cancer Control* 2008;15:233–8. [PubMed: 18596675]
45. McWilliams RR, Brown PD, Buckern JC, et al. Treatment of brain metastases from melanoma. *Mayo Clin Proc* 2003;78:1529–36. [PubMed: 14661682]
46. Wolf M, Eskerski H, Bauder-Wust U, Haberkorn U, Eisenhut M. Alkylating benzamides with melanoma cytotoxicity: experimental chemotherapy in mouse melanoma model. *Melanoma Res* 2006;16:487–96. [PubMed: 17119449]
47. Desbois N, Gardette M, Papon J, et al. Design, synthesis and preliminary biological evaluation of acridine compounds as potential agents for a combined targeted chemo-radionuclide therapy approach to melanoma. *Bioorgan Med Chem* 2008;16:7671–90.
48. Miao Y, Owen NK, Fischer DR, et al. Therapeutic efficacy of a (188)Re-labeled alpha-melanocyte-stimulating hormone peptide analog in murine and human melanoma-bearing mouse models. *J Nucl Med* 2005;46:121–9. [PubMed: 15632042]
49. Dadachova E, Nosanchuk JD, Shi L, et al. Dead cells in melanoma tumors provide abundant antigen for targeted delivery of ionizing radiation by a mAb to melanin. *P Natl Acad Sci USA* 2004;101:14865–70.
50. Dadachova E, Revskaya E, Sesay MA, et al. Pre-clinical evaluation and efficacy studies of a melanin-binding IgM antibody labeled with (188)Re against experimental human metastatic melanoma in nude mice. *Cancer Biol Ther* 2008;7:1116–27. [PubMed: 18535406]

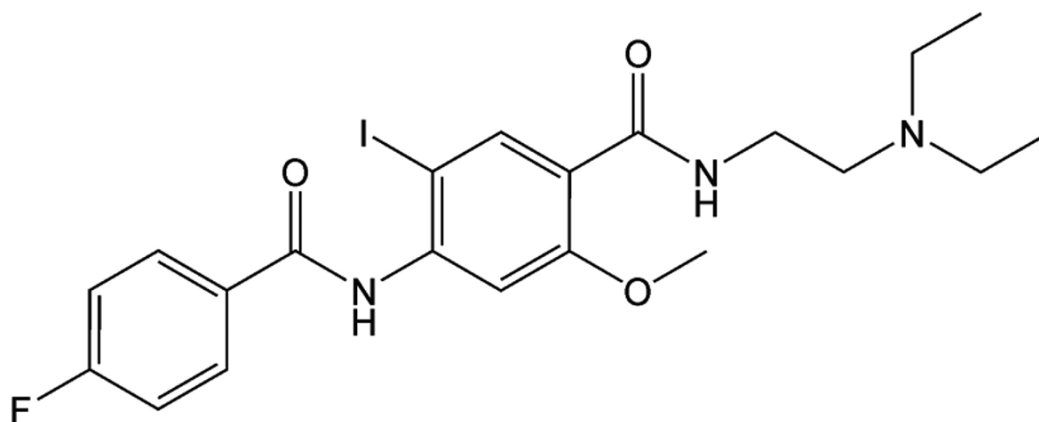


Figure 1.
Structure of MIP-1145.

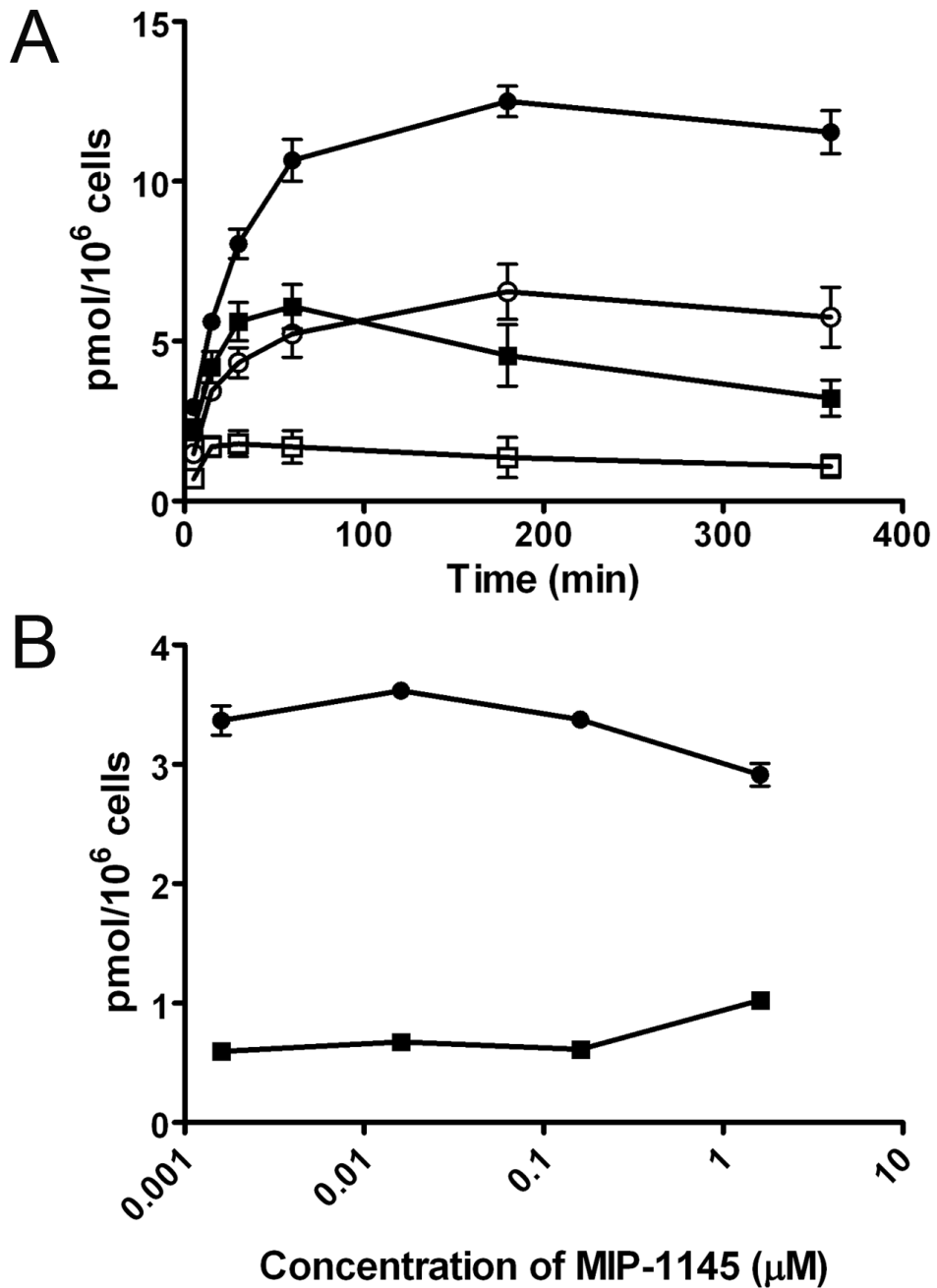


Figure 2. Binding of [¹³¹I]MIP-1145 to human melanoma SK-MEL-3 and A375 cells. **A.** SK-MEL-3 and A375 cells were incubated with 11.5 nM [¹³¹I]MIP-1145 for up to 6 hours at 37 °C. The medium was removed, the cells were washed with (SK-MEL-3 ○, A375 □) or without (SK-MEL-3 ●, A375 ■) a mild acid solution, and counted in a gamma counter. **B.** SK-MEL-3 ● and A375 ■ cells were incubated with 3.6 nM [¹³¹I]MIP-1145 for 2 hours with increasing amounts of non-radiolabeled MIP-1145.

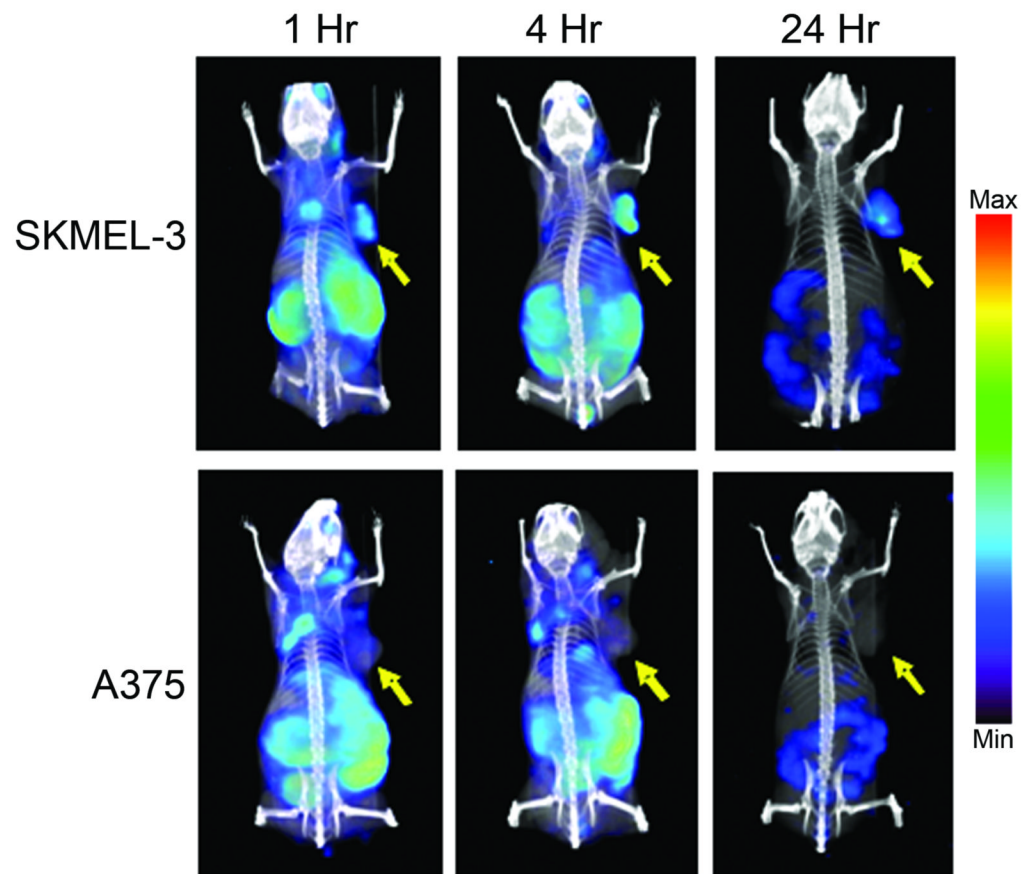


Figure 3. SPECT/CT imaging of [^{123}I]MIP-1145 in nude mice bearing human melanoma SK-MEL-3 and A375 xenografts, at 1, 4, and 24 hours post-injection. Arrows indicate tumor.

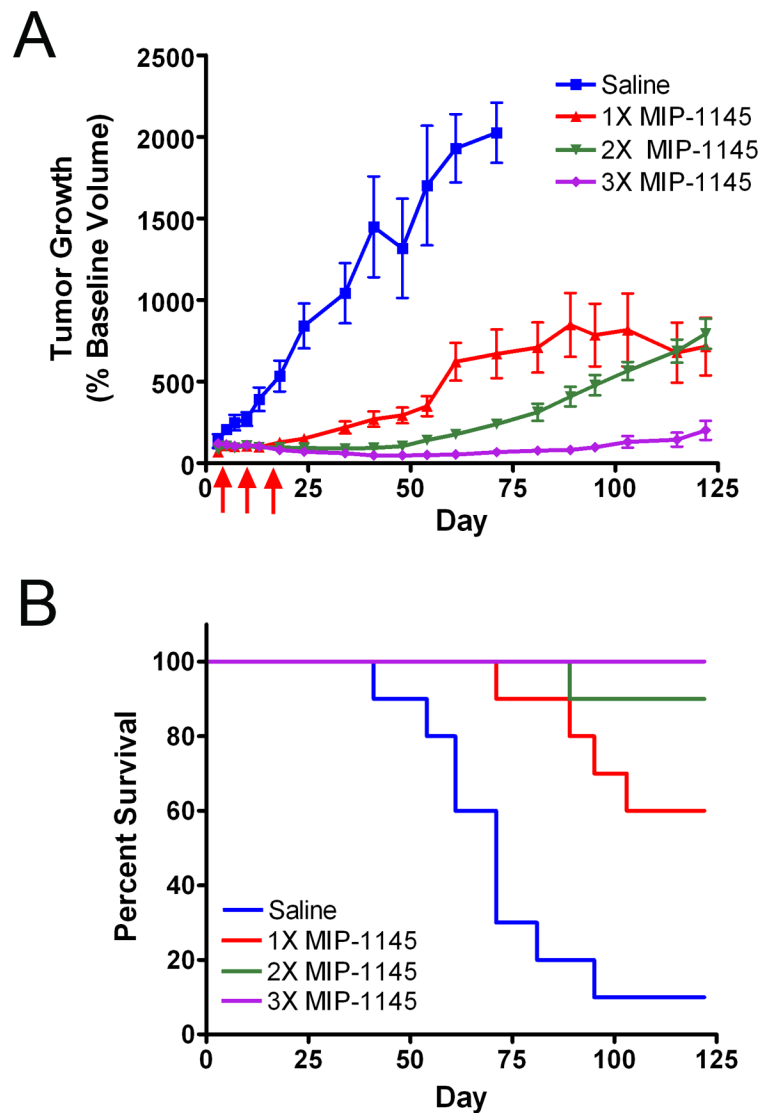


Figure 4. Effect of [¹³¹I]MIP-1145 on **A.** human melanoma SK-MEL-3 tumor growth and **B.** animal survival. [¹³¹I]MIP-1145 was administered at 2.5 GBq/m² either as a single dose, or once weekly for 2 weeks, or once weekly for 3 weeks. Arrows indicate treatment days. Tumor growth data are expressed as the percent change in tumor volume relative to baseline. Survival in each group was calculated as the number of animals that remained in each group at indicated times (animals either died naturally with tumor or were sacrificed when tumors reached 1,500 mm³).

Table I
Tissue distribution of [¹³¹I]MIP-1145 in SK-MEL-3 and A375 xenografts (%ID/g, mean ± SD)

SKMEL-3	Time (hours)		
	1	4	24
Blood	0.75 ± 0.12	0.35 ± 0.04	0.03 ± 0.00
Heart	2.36 ± 0.18	1.32 ± 0.18	0.04 ± 0.03
Lungs	9.70 ± 1.28	6.87 ± 1.33	0.29 ± 0.08
Liver	7.94 ± 1.12	5.18 ± 0.59	0.50 ± 0.07
Spleen	7.26 ± 1.18	3.75 ± 0.60	0.12 ± 0.03
Kidneys	16.55 ± 0.52	13.12 ± 2.68	0.51 ± 0.18
Stomach	12.85 ± 2.53	10.74 ± 2.52	1.41 ± 0.53
Large Intestine	2.93 ± 0.54	18.91 ± 3.84	2.24 ± 0.67
Small Intestine	15.19 ± 1.50	17.21 ± 2.05	1.03 ± 0.24
Testes	1.51 ± 0.18	1.07 ± 0.09	0.22 ± 0.02
Skeletal Muscle	1.39 ± 0.16	0.73 ± 0.16	0.03 ± 0.02
Bone	1.71 ± 0.28	0.95 ± 0.14	0.09 ± 0.08
Brain	0.82 ± 0.06	0.19 ± 0.02	0.01 ± 0.01
Adipose	4.15 ± 2.89	1.03 ± 0.26	0.09 ± 0.05
Tumor	3.77 ± 1.68	8.82 ± 3.55	5.91 ± 3.94
A375	Time (hours)		
	1	4	24
Blood	0.46 ± 0.05	0.26 ± 0.04	0.04 ± 0.02
Heart	1.96 ± 0.33	1.04 ± 0.06	0.02 ± 0.02
Lungs	9.81 ± 0.88	7.24 ± 1.31	0.37 ± 0.15
Liver	6.79 ± 1.33	4.30 ± 0.45	0.32 ± 0.06
Spleen	4.54 ± 1.34	2.57 ± 0.51	0.15 ± 0.20
Kidneys	14.26 ± 2.73	8.53 ± 1.20	0.21 ± 0.08
Stomach	6.22 ± 2.34	4.57 ± 1.77	0.67 ± 0.27
Large Intestine	2.69 ± 0.49	13.81 ± 5.14	1.35 ± 0.36
Small Intestine	9.19 ± 3.32	12.44 ± 2.02	0.59 ± 0.24
Testes	1.58 ± 0.22	0.90 ± 0.13	0.16 ± 0.05
Skeletal Muscle	1.03 ± 0.09	0.58 ± 0.12	0.02 ± 0.01
Bone	1.34 ± 0.12	0.74 ± 0.07	0.03 ± 0.02
Brain	0.60 ± 0.17	0.16 ± 0.01	0.01 ± 0.00
Adipose	1.56 ± 0.23	1.10 ± 0.46	0.13 ± 0.12
Tumor	2.38 ± 0.75	1.19 ± 0.07	0.04 ± 0.02

Table II
Projected human organ radiation absorbed dose extrapolated from the cynomolgus monkeys (mGy/MBq, mean \pm SD)

Adrenals	8.50E-02 \pm 1.80E-02
Brain	7.00E-02 \pm 1.50E-02
Breasts	6.40E-02 \pm 1.40E-02
Eyes	1.30E+00 \pm 6.70E-01
Gallbladder Wall	1.20E-01 \pm 1.90E-02
LLI Wall	2.80E+00 \pm 1.80E-02
Small Intestine	3.40E-01 \pm 1.80E-02
Stomach Wall	9.80E-02 \pm 1.80E-02
ULI Wall	1.10E+00 \pm 1.50E-02
Heart Wall	8.00E-02 \pm 1.80E-02
Kidneys	1.10E-01 \pm 7.70E-02
Liver	8.60E-02 \pm 1.70E-02
Lungs	6.70E-02 \pm 2.00E-02
Muscle	8.80E-02 \pm 1.60E-02
Ovaries	2.00E-01 \pm 1.90E-02
Pancreas	9.20E-02 \pm 1.90E-02
Red Marrow	8.70E-02 \pm 1.40E-02
Osteogenic Cells	1.60E-01 \pm 3.30E-02
Skin	6.60E-02 \pm 1.40E-02
Spleen	8.50E-02 \pm 1.80E-02
Testes	8.60E-02 \pm 1.60E-02
Thymus	7.80E-02 \pm 1.70E-02
Thyroid	1.80E+01 \pm 1.30E+01
Urinary Bladder Wall	6.20E-01 \pm 4.10E-02
Uterus	1.50E-01 \pm 1.80E-02
Total Body	1.00E-01 \pm 1.60E-02
Effective Dose Equivalent	9.20E-01 \pm 3.70E-01
Effective Dose	1.40E+00 \pm 6.30E-01